Residual stress determination by blind hole drilling and local displacement mapping in aluminium alloy aerospace components

Sviatoslav Eleonsky, Vladimir Pisarev
The Zhukovsky Central Aero-Hydrodynamics Institute (TsAGI), 140180 Zhukovsky, Moscow Region, Russia
juzzepka@mail.ru, https://orcid.org/0000-0003-4345-067X
VSP5335@mail.ru, https://orcid.org/0000-0002-5378-609X

Eugene S. Statnik, Alexey I. Salimon
HSM lab, Center for Digital Engineering, Skoltech, 121205 Moscow, Russia
eugene.statnik@skoltech.ru, https://orcid.org/0000-0002-1105-9206
a.salimon@skoltech.ru, https://orcid.org/0000-0002-9048-8083

Alexander M. Korsunsky
Independent researcher
alexander.korsunsky@gmail.com, https://orcid.org/0000-0002-3558-5198

Frattura ed Integrità Strutturale – Fracture and Structural Integrity

Visual Abstract

Residual stress determination by blind hole drilling and local displacement mapping in aluminium alloy aerospace components

Sviatoslav Eleonsky, Vladimir Pisarev
The Zhukovsky Central Aero-Hydrodynamics Institute (TsAGI) Eugene S. Statnik, Alexey I. Salimon
HSM lab, Center for Digital Engineering, Skoltech
Alexander M. Korsunsky
Independent researcher (Principle investigator)

KEYWORDS. Residual stress, Blind hole drilling method, Speckle-pattern interferometry, Well-posed inverse correlation problem

INTRODUCTION

Residual stress significantly impacts the mechanical performance of structural materials, including plastic deformation, surface integrity crack initiation, and ultimate strength. For instance, the presence of tensile residual stress can reduce the material performance and component life, whereas residual compressive stress may enhance material fatigue strength. Despite being "hidden" in the absence of external loads, residual stresses play a crucial role in the

material deformation behavior [1]. They are inherent in most manufacturing processes, including plastic deformation, welding, heat treatment, machining, and 3D printing. These processes alter the shape and affect the mechanical properties of materials. However, in many cases, it is difficult to pinpoint the source of the residual stresses and accurately track their evolution. This poses challenges for reliable computer modeling of the mechanical response in numerical simulations. Thermo-mechanical deformation modelling requires the knowledge of a significant number of unknown parameters. Unknown residual stresses, alongside micro-structural modification, pose a significant obstacle to using advanced welded structures in diverse industrial sectors. The incorporation of predictive residual stress analysis into design requires high-fidelity experimental data to obtain reliable service life prognosis. This necessity is particularly significant in the aerospace, nuclear, and other critical industries [1,2].

The nature and origins of numerous experimental and theoretical challenges that exist in measuring residual stress are well described in references [3-5]. The present article discusses using the blind hole drilling technique coupled with ESPI to estimate the residual stress in thick-walled structures. The hole drilling method is one of the most effective and extensively deployed experimental techniques to characterize residual stresses. The rapid advancement and implementation of optical interferometric techniques have facilitated the contactless measurement of local displacement fields on metallic surfaces of real objects, thereby presenting innovative prospects for hole drilling residual stress measurements. Multiple studies have focused on combining the hole drilling method with full-field measurement techniques based on optical interferometry. Comprehensive overviews of the current state of the art in the field of combining the hole-drilling method with optical interferometric measurements of the local deformation response for residual stress determination are presented in papers [6-10].

Additional applications of blind hole drilling to residual stress characterization are available elsewhere [11-29]. In general, the determination of residual stresses from strain relief experimental data constitutes an inverse problem. It is noted, in passing, that in this context the term "relaxation" is often used incorrectly, as it implies the action of inelastic deformation mechanism(s), such as creep – therefore, the term "relief" is preferred in reference to local, predominantly elastic unloading. Any method used to evaluate the residual stress through strain relief assumes that the values of measured parameters (displacements or strains) caused by local material removal are solutions of an integral equation that must be inverted to determine the residual stresses [21, 30-32]. In practice, stress distributions are represented on a finite-dimensional basis, thus transforming the integral equations into a system of linear algebraic equations. However, this system is frequently ill-conditioned. In the general case, the determination of residual stress necessitates solving an ill-posed inverse problem, as discussed in [32]. However, a viable solution to circumvent the challenges associated with ill-posed problems is to convert them into a well–posed inverse problem [30]. This can be achieved by employing a suitable measurement procedure, e.g., estimating the hole diameter increments in the principal strain directions [10]. In this case, the explicit form of the direct solution, connecting the stress values and measured parameters, has been derived [33, 34].

The present research study employs a systematic approach and demonstrates its advantages by considering two cases of real engineering parts utilized in civil aircraft construction. The initial investigation of residual stress characterization involves a simulated section of a lower wing panel for commercial civil aircraft. This section is notably thick and includes a stringer with a mesh of holes to facilitate assembly manipulations. Residual stress is induced through a series of operation-fatigue tests, removal of bolts, and skin separation from the stringer. These stress data are valuable for predicting and analyzing the fatigue strength of the structure. The second case examines the residual stress components near holes hardened by the StressWaveTM method developed by Stress Wave Inc. (Kent, WA, USA) [35, 36]. The first step of the StressWaveTM process involves placing the object between hardened indenters to transmit the stress wave into the target metal, forming a small dimple on each side of the work piece. The metal flows plastically in a radial direction from the indenters entrapping the material between them, leading to the uniform residual stress distribution within an isotropic material. The plastic flow results in cold working of the surrounding hole area. The subsequent step involves drilling the hole, removing the entire dimple and much or all of the surface upset caused during the process. Although the StressWaveTM process generates residual stresses through cold working via a stress wave, it is important to note that the process is dynamic. In certain positions, local material volumes may experience loading ranging from quasi-static to unstable dynamic characteristics across a range of strain rates.

Residual stress estimation was first conducted near a hole treated by the StressWaveTM technique in 7075-T651 aluminum alloy by using the neutron diffraction method [35]. Next, residual stress determination around a cold-expanded hole in 7075-T73 aluminum alloy was carried out using the Sachs' method [37]. The study revealed that the StressWave® technique significantly improves the life factor relative to a plain hole exceeding values for Split Sleeve technique [38]. On the other hand, to the best of the author's knowledge, there is no quantitative data on the distribution of residual stress obtained by the drilling method for a hole treated with the StressWaveTM technique.

In recent years, there has been increasing interest in metal additive manufacturing or metal 3D printing. Both these processes lead to residual stress arising at the micro- and meso-structure level [38, 39]. Capabilities of blind hole drilling and interferometric measurements of deformation response have been previously demonstrated in the course of residual stress quantifying in 3D printed specimens [29]. A set of experimental difficulties was revealed. One of perspective goals of present research is connected with the refinement of nuances of experimental procedure in relation to residual stress characterization in additive materials.

The drilling of deep blind holes results in the release of elastic energy from residual stress, leading to the deformation of the theoretically circular contour of the hole. Monitoring the deformation response is done using ESPI. High-quality interferogram sets, which offer a reliable resolution of interference fringes to quantify hole diameter increments along principal residual strain directions, have been acquired. The solution to a well-conditioned system of linear algebraic equations is utilized to derive the principal residual stress components.

OBJECTS OF INVESTIGATION

The evaluation of residual stress levels in structural elements after fatigue test is vital for validating reliable service life predictions using numerical simulation methods. This is particularly crucial for samples that contain irregular stress concentration regions. In this paper, two samples with different shapes and an extensive processing history were selected. The first sample was defined as a considerably thick specimen, while the second one was referred to a specimen with intermediate thickness.

T-shaped Sample 1

The first specimen was a significantly thick element with a series of perforations, replicating a rib segment that is a part of a civil aircraft's lower wing panel. This panel with a size of 3700×560 mm in plane, which consists of external skin reinforced by two longitudinal ribs (stringers), was fabricated from 2024 aluminum alloy (E = 74 GPa, σ_y = 330 MPa, ν = 0.33).

The skin and stringers were connected together using bolts. Prior to joining, cold expansion was carried out on holes that were drilled in both the skin and stringers with 0.5 % interference. Then, the steel bolts were mounted with an interference fit ranging from 1.3 % to 2.1 %, due to overlapping of the tolerance fields in the bolts and assemblage hole diameters. The assembly of skin-stringer, representing comparably designed model, was subjected to cyclic loading in order to obtain data essential for fatigue strength analysis, taking into account residual stress influence. The fatigue test, which involved cyclic tension, was conducted under the specified parameters: stress range of $\Delta\sigma$ = 160 MPa and stress ratio R = 0.01. The direction of pulsing tensile load applied during the fatigue test coincides with the stringer axis. The test was terminated if and when it exceeded 130000 cycles without any failures.

Then, the ends of skin-stringer assembly were cut from the middle to separate uniformly loaded tested element. After, the bolted joints were demounted, and the stringer was detached from the skin. The T-shaped stringer fragment with the dimensions of 215×122×15 mm (Fig. 1(a)) was used to experimentally determine the principal residual stress components. The general view of this fragment with the indication of probe area on the external surface as a red rectangular is shown in Fig. 1(a). The geometrical details of the experiment, including the probe hole grid with the drilling order and step size in both directions, can be found in Fig 1(b).

Sample 2 with strengthened open hole

The second specimen was an aluminium (E = 72 GPa, σ_y = 300 MPa, ν = 0.33) rectangular plate with the dimensions of 150×50×10 mm as shown in Fig. 2 (a). In this case, residual stresses were analyzed in the vicinity of the holes strengthened using StressWaveTM method developed by Stress Wave Inc. (Kent, WA, USA). This method relies on locally strengthening the material by compressing two symmetric punches with semi-spherical ends, resulting in the creation of uniform and significantly large zones of compressive residual stresses in metals. The StressWaveTM process steps are illustrated in Fig. 2 (b), 2 (c) and 2 (d). The process assumes the introduction of compressive residual stresses prior to drilling, without any additional processing operations. Hardened indenters create plastic strains in an area smaller than the diameter of the subsequently drilled hole. The introduction of uniform residual stresses in the thickness direction is indicated by small dimples on both sides of the work-piece with a diameter slightly smaller than that of the drilled hole during the first phase of the StressWaveTM process. The process has been employed in diverse alloys such as aluminium, steel, titanium, and cast iron, and for section thickness ranging from 0.8 to 25 mm.

In this study, two symmetrically applied indenters made of 16 mm hardened steel balls were used to create plastically induced dimples. The 70 kN external force generated a 6.0 mm plastic dimples while the drilling of a 6.2 mm hole entirely removed the curved dimples surfaces.
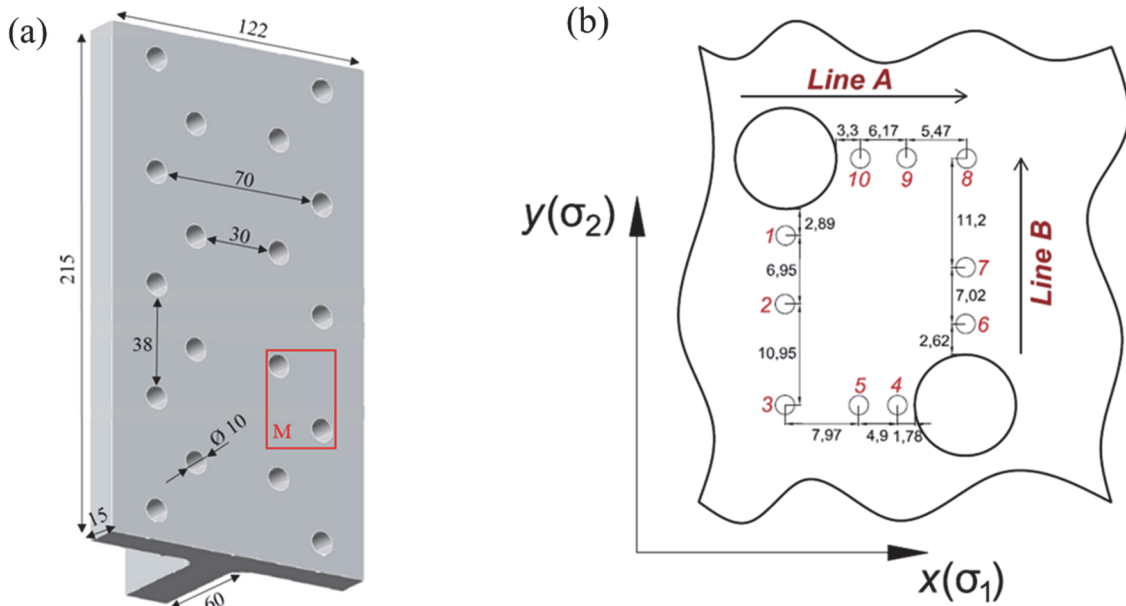

Figure 1: (a) The appearance of the T-shaped stringer part. (b) The experimental grid of probe holes in M area with the indication of coordinate system.
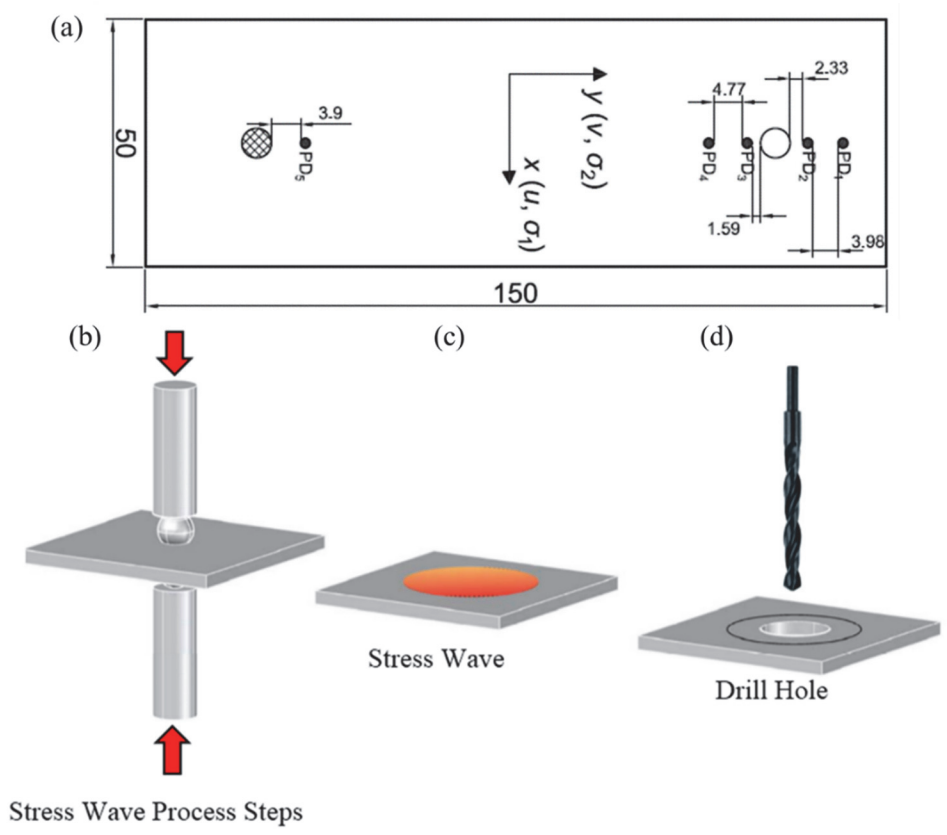

Figure 2: (a) (a) The sketch of the second specimen with indication of its size, dimples and probe holes locations, and coordinate system. (b-d) The StressWaveTM process of compressive residual stresses formation.

EXPERIMENTAL PROCEDURE

The Electronic Speckle-Pattern Interferometry (ESPI) technique was applied to measure the hole diameter increments (Δu and Δv in the principal stress directions) resulting from the release of elastic energy of residual stresses caused by removal of stressed material during hole drilling. Optical system with normal illumination with respect to the plane object surface and two symmetrical observation directions was applied. Compact diode laser having wavelength $\lambda = 532$ nm was the source of the coherent light illumination to obtain interference fringe patterns in a fast and reliable manner after blind hole drilling. The details of experimental procedure are given in article [10]. In this study, probe holes were made using a hard-coated drill with a 1.9 mm diameter ($2 r_0$). The blind hole depth (h) in all cases met the condition of $h \geq 3 r_0$.

Initial parameters extraction

The first experimental step employs obtaining high-quality interference fringe patterns, which arise after local material removal. Typical interference fringe patterns (so-called interferograms) obtained for T-shaped stringer fragment are illustrated in Fig. 3.
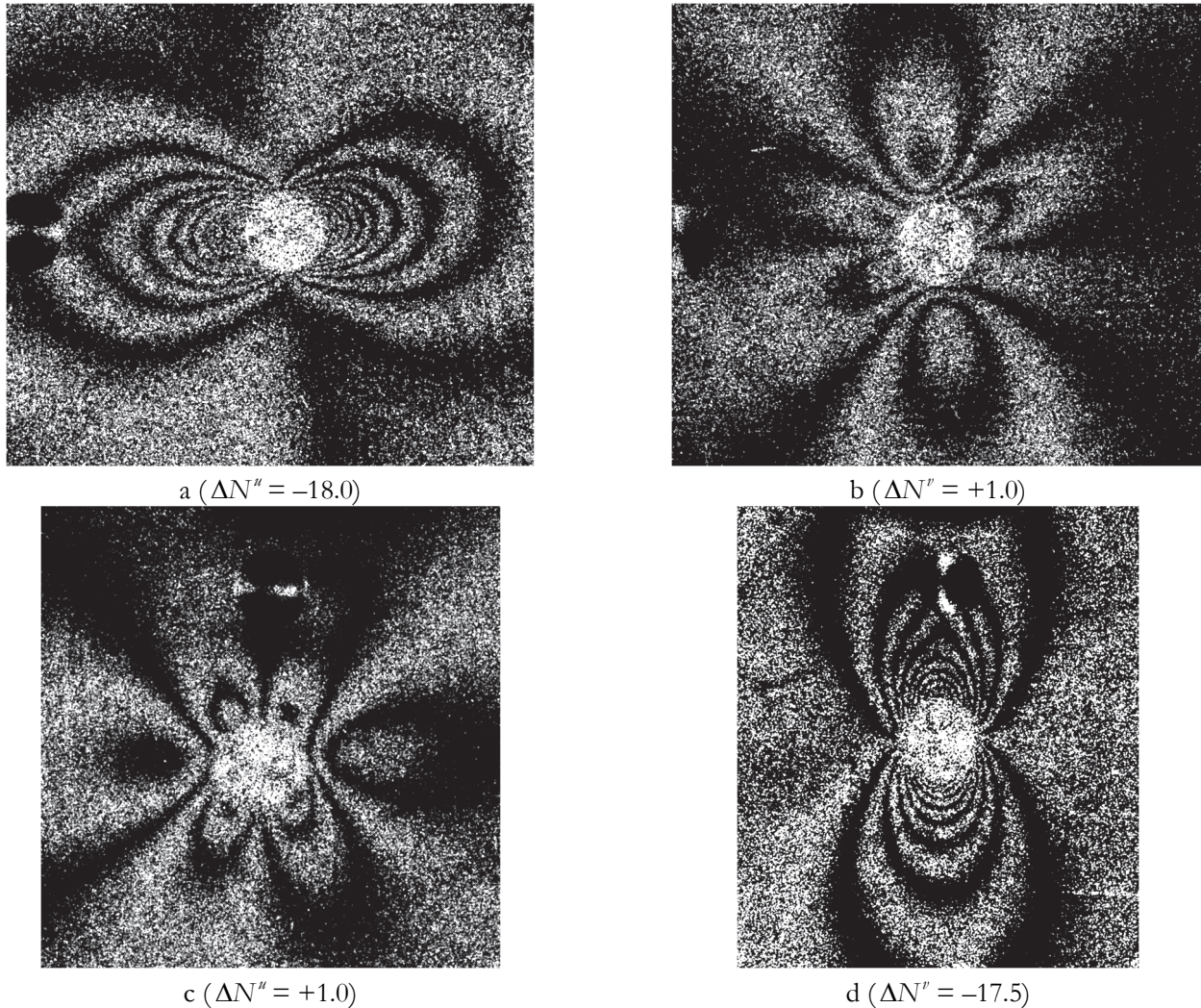

a ($\Delta N^u = -18.0$) b ($\Delta N^v = +1.0$)

c ($\Delta N^u = +1.0$) d ($\Delta N^v = -17.5$)

Figure 3: The interference fringe patterns obtained for in-plane displacement component u (a,c) and v (b,d) as the result of blind hole drilling at point 2 (a, b) and 5 (c, d) for Sample 1.

Typical interferograms obtained in the vicinity of the strengthened hole are shown in Fig. 4.
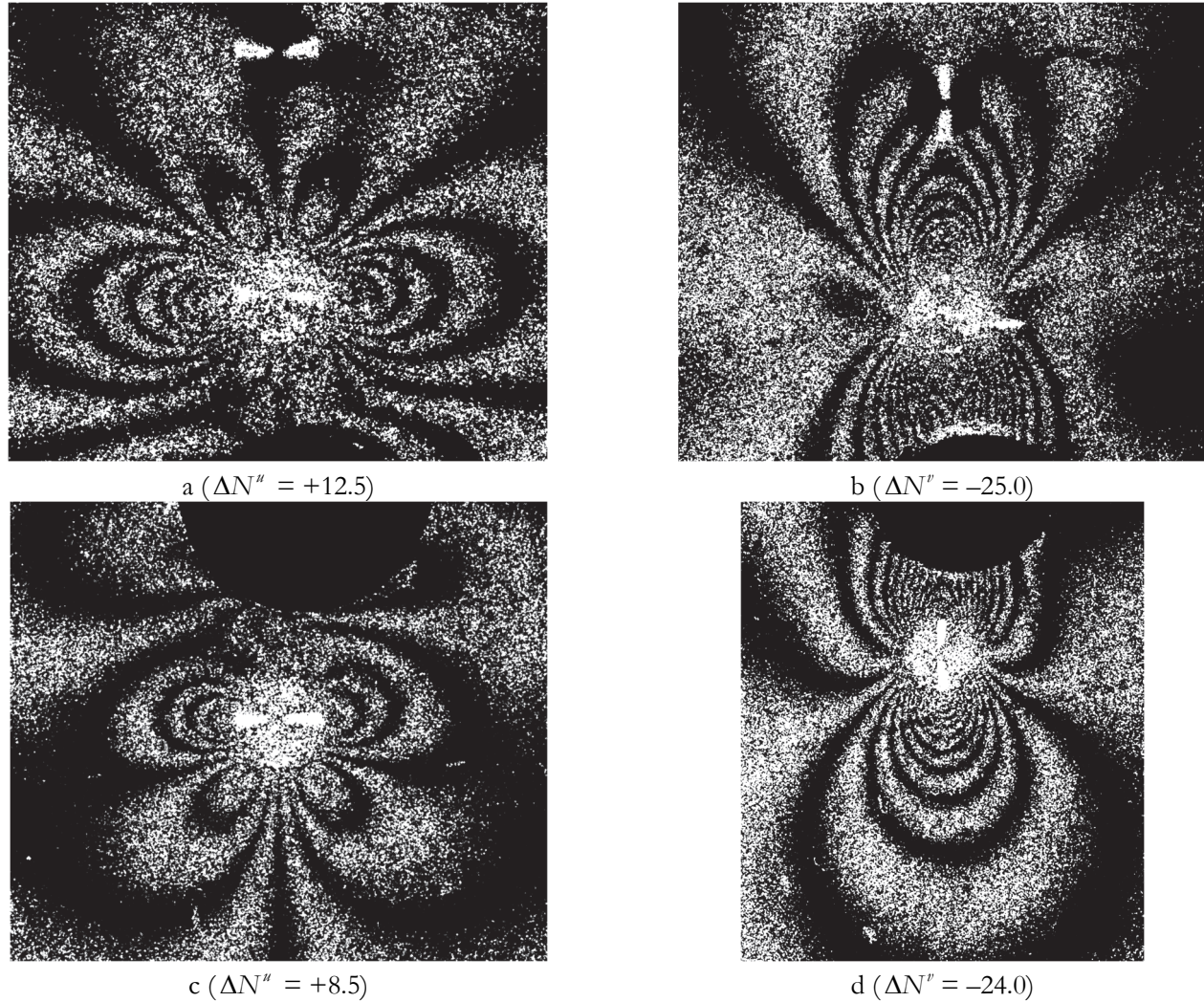
a ($\Delta N^u = +12.5$)

b ($\Delta N^v = -25.0$)

c ($\Delta N^u = +8.5$)

d ($\Delta N^v = -24.0$)

Figure 4: The interference fringe patterns obtained for in-plane displacement component u (a, c) and v (b, d) as the result of blind hole drilling at point 2 (a, b) and point PD2 (a, b) and PD3 (c, d) for Sample 2.

The second step resides in deriving hole diameter increments in principal stress directions (Δu and Δv), which are essential for further residual stress calculations. It is of importance that the acquired interferograms exhibit exceptional quality for the subsequent post-processing. The fringe patterns depicted in Figs. 3 (a), 3 (d) and 4 (d), 4 (d) reveal 18.0, 17.5 and 25.0, 24.0 fringes over the boundary of 1.9 mm hole diameter. Furthermore, they show that the coordinate axes x and y closely coincide with the direction of principal residual stress components σ_1 and σ_2, respectively. This means that Δu and Δv values follows from the main relations of ESPI method [10]:

$$\Delta u = \Delta N^u \frac{\lambda}{2\sin\psi}, \quad \Delta v = \Delta N^v \frac{\lambda}{2\sin\psi}, \tag{1}$$

where λ is wavelength of laser illumination (532 nm), ψ is angle between inclined illumination and normal observation directions ($\pi/4$), ΔN^u and ΔN^v are differences between absolute fringe orders counted over the solitary fringe pattern between two basic points corresponding to the directions of principal stresses σ_1 and σ_2, respectively.

In this study, two basic points corresponding to each fringe pattern were defined as the intersection points of the hole diameter coinciding with a specific principal stress direction and the edge of the probe hole. The horizontal and vertical diameters are related to the ΔN^u and ΔN^v absolute fringe order difference, respectively.

Brief illustration of this process follows below by employing two interferograms with relatively low fringe density, shown in Fig. 5, to clarify the essence of involved procedure. The required values of hole diameter increments Δu and Δv could be obtained from Eqns. (1) by directly counting fringe orders ΔN^u and ΔN^v between two basic points on the fringe patterns. Basic points, shown in Fig. 5, are denoted as 1* and 2* for u–displacement component as well as 3* and 4* for v–displacement component. The way of fringe order difference counting is shown in Fig. 5 (a) and 5 (b) for ΔN^u and ΔN^v, respectively.
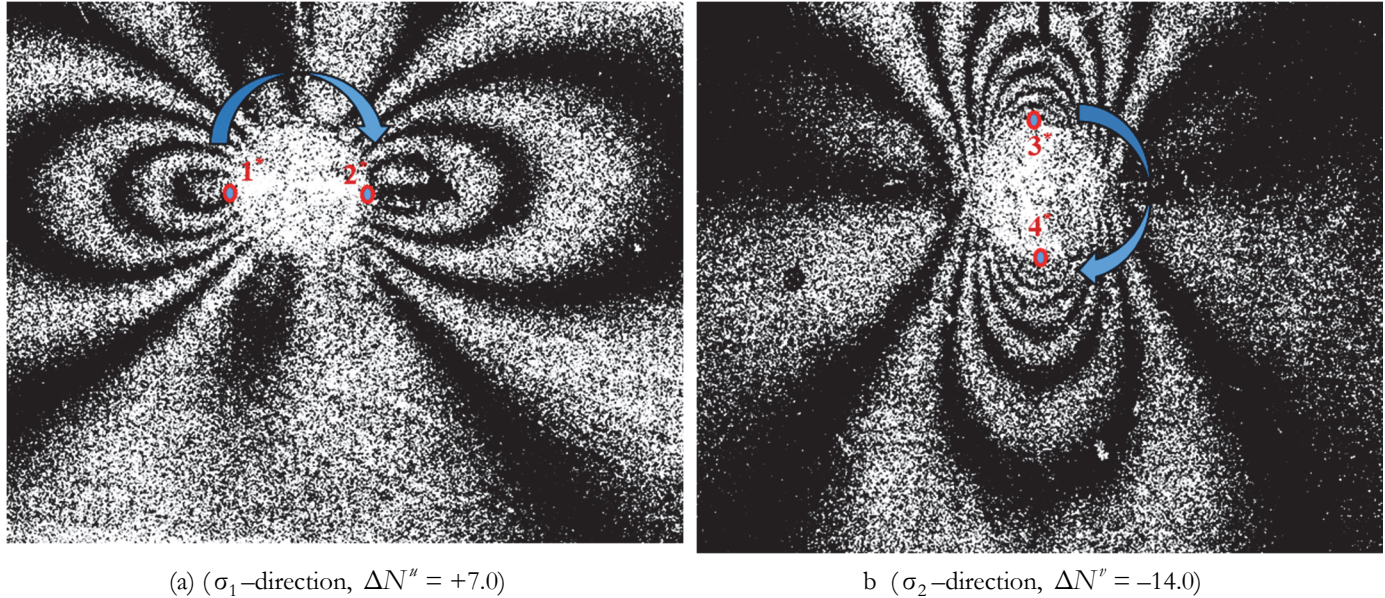

(a) (σ_1–direction, $\Delta N^u = +7.0$)   b (σ_2–direction, $\Delta N^v = -14.0$)

Figure 5: General scheme of fringe order differences deriving.

Initial parameters extraction

Coinciding symmetry axes of obtained interferograms and directions of principal residual stress components proves that the determination of residual stress can rely on the approach described in study [10]:

$$\sigma_1 = \frac{E}{2r_0}\left\{\frac{a\Delta u + b\Delta v}{a^2 - b^2}\right\}, \quad \sigma_2 = \frac{E}{2r_0}\left\{\frac{a\Delta v + b\Delta u}{a^2 - b^2}\right\}, a = \alpha_1 - 1, \; b = \alpha_2 - \mu, \tag{2}$$

where r_0 is hole radius, E is Young's modulus of the material, Δu and Δv are hole diameter increments in principal stress directions σ_1 and σ_2, respectively, α_1 and α_2 are strain concentration factors, μ is Poisson's ratio of the material.

In the case involved, let us assume that $\alpha_1 = 3$ and $\alpha_2 = 1$ because these values satisfy to the numerical solution of the elastic stress concentration problem for uniaxial tension of thick plate with deep blind hole when the condition of $h \geq 3r_0$ is met [23]. To calculate residual stress using Eqns. (2), it is necessary to determine the diameter increments of the hole in the directions of principal stress (Δu and Δv) accordingly to formulae (1).

Deriving accurate residual stress values from Eqns. (2) requires identifying a sign of the hole diameter increment Δu and Δv (increase or decrease) as described in formula (1). The challenge arises because interference fringe patterns, like those illustrated in Fig. 3 and Fig. 4, do not inherently provide information on the exact physical orientation of each displacement component. To obtain the necessary data to determine the plus or minus sign of each in-plane displacement component, an additional phase shift can be introduced before the second exposure during interferogram recording. The sign of a particular phase shift is typically known in advance for a given interferometer optical system. This technique facilitates the identification of the physical orientation of each in-plane displacement component for each specific configuration of the optical system. Interferograms similar to those presented in Figs. 3c and 3d, but recorded with an added constant phase shift for physical orientation identification, are shown in Fig. 6. As demonstrated in Fig. 6(a), the optical system generates a hyperbolic fringe pattern for a positive sign of component u, while a negative sign of component v produces an elliptical fringe pattern, as shown in Fig. 6(b).

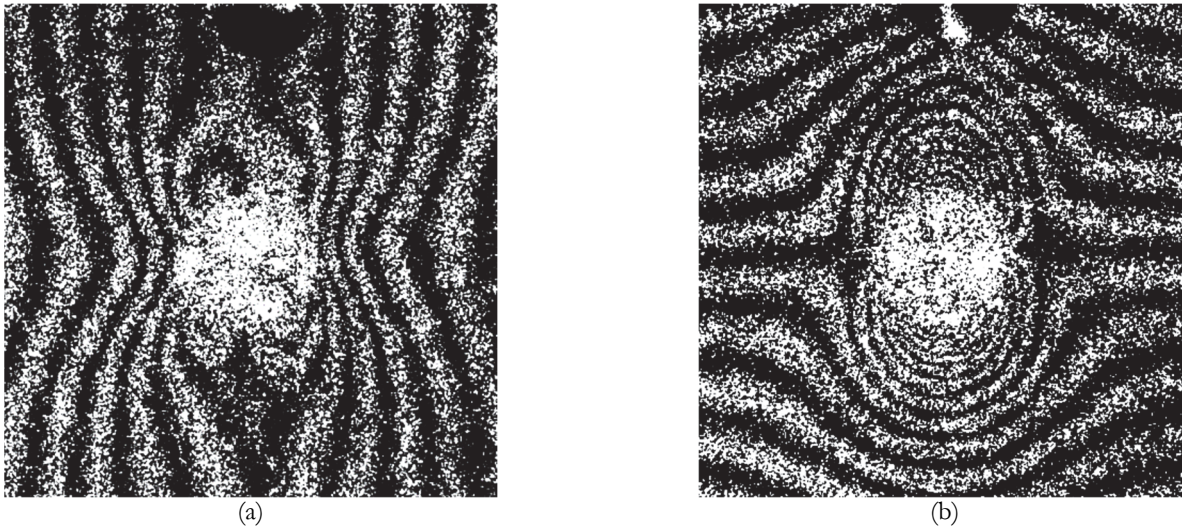(a)   (b)

Figure 6: Interference fringe patterns obtained with the additional phase shift for in-plane displacement component u (a) and v (b) as the result of hole drilling.

UNCERTAINTY ANALYSIS

A satisfactory correlation between the actual residual stress state and transition model (1) provides an opportunity to quantitatively estimate the uncertainties in measured residual stress values. Our proposed approach is based on the matrix formulation of the problem of residual stress determination using formulae (1). Initially, the vector s should be composed of two unknown parameters σ_1 and σ_2:

$$s = \{\sigma_1, \sigma_2\}^T \tag{3}$$

At the same time, the effect vector d should include determined experimental parameters Δu and Δv:

$$d = \{\Delta u, \Delta v\}^T \tag{4}$$

The equation below connects vectors s and d as

$$A \cdot s = d \tag{5}$$

where A is the explicit form of the transition model [10, 23, 33, 34, 40].
According to the Eqn. (5), the required vector s can be obtained through an inverse problem solution [30]:

$$s = A^{-1} \cdot d \tag{6}$$

Hence, if a length of vector s is equal to $n = 2$, then a dimension of matrix A from Eqn. (5) is $[n \times n] = [2 \times 2]$. On the other hand, if matrix A is a regular positively defined square $[n \times n]$-matrix, the problem is properly posed and the unequivocally solution of Eqn. (6) exists [30]. The elements of the mentioned above matrix A for the effect vector d of form (4) can be constructed from general formulae derived in work [34]:

$$a_{11} = a_{22} = \frac{2r_0}{E(\alpha_1 - 1)}, \ a_{21} = a_{12} = \frac{2r_0}{E(\alpha_2 - \mu)} \tag{7}$$

It is evident that a solution of Eqn. (6) for matrix A of type (7) gives formulae (1). However, employing a problem formulation that includes relations (3)-(7) also allows for quantifying uncertainties for principal residual stress components. This can be accomplished following the general approach outlined in reference [34]. Required estimations stem from the mathematical formulation of the direct problem (5), and can be performed precisely if the form of matrix A is known with high degree of reliability as it takes place for the case considered. The upper limit of the calculation error for each component of unknown vector s can be estimated as following:

$$\frac{\left|\delta s_i\right|}{s} \leq \frac{cond\{A\}}{2} \frac{\left|\delta d_i\right|}{d} \tag{8}$$

where $i = 1,2$; $\left|\delta s_i\right|$ and $\left|\delta d_i\right|$ are the errors made in the determination of s_i and d_i components; $cond\{A\} = A \cdot A^{-1}$ is the condition number of matrix A [42].

The symbol $*$ denotes the vector and matrix norm. The formulation of inequality (8) considers that all rows of matrix A (7) are of equal length. Vector norms included in Eqn. (6) are defined as a length of corresponding vector $s = \sqrt{s_1^2 + s_2^2}$, etc. Matrix norm that is equivalent to this vector norm is Euclid norm:

$$A = \left\{ \sum_{i,j} \left|a_{i,j}\right|^2 \right\}^{1/2} \tag{9}$$

where $a_{i,j}$ are the elements of arbitrary matrix A.

The value of Euclid norm for matrix A (7) directly follows from definition (9):

$$A = \sqrt{2} \cdot \sqrt{a^2 + b^2} \tag{10}$$

where $a = \alpha_1 - 1$ and $b = \alpha_2 - \mu$.

Comparison of relations (1) and (7) provides the form of inverse matrix A^{-1}:

$$A^{-1} = \frac{1}{a^2 - b^2} \begin{bmatrix} a & b \\ b & a \end{bmatrix} \tag{11}$$

Euclid norm (10) of matrix of type (11) has the following form:

$$A^{-1} = \frac{\sqrt{2} \cdot \sqrt{a^2 + b^2}}{a^2 - b^2} \tag{12}$$

The value of condition number for matrix A of type (7) is defined by multiplying relations (10) and (12):

$$cond\{A\} = 2\frac{a^2 + b^2}{a^2 - b^2} \tag{13}$$

Relation (13) evidences that the value of the condition number for the approach involved cannot be less than 2. For the case considered in this report, we assumed that $a = 2$, $b = 0.67$, and $cond\{A\} = 2.51$.

The quantitative estimation of errors in residual stress calculations is evidently linked with the experimental errors in the Δu and Δv increments of probe hole diameter, as determined by formulae (2), ultimately yielding formulae (14):

$$\delta\left(\left|\Delta u\right|\right) \le \delta\left(\left|\Delta N^{u}\right|\right)\frac{\lambda}{2\sin\psi}, \quad \delta\left(\left|\Delta v\right|\right) \le \delta\left(\left|\Delta N^{v}\right|\right)\frac{\lambda}{2\sin\psi} \tag{14}$$

The approach presented in this paper is based on experimental determination of two exclusive parameters, namely, the two differences between fringe orders on external face of the specimen. These values are derived for a single fringe pattern between a pair of basic points located at the hole edge. In this work, the required fringe counts were obtained manually via "naked-eye" observations performed by an operator. Quantitative uncertainty analysis based on inequality (8) employs $\left|\delta d_{i}\right|$ parameter. The first step in this way resides in obtaining $\delta\left(\left|\Delta u\right|\right)$ and $\delta\left(\left|\Delta v\right|\right)$ values from inequalities (14). The accuracy analysis of all experimental results assumes determination the fringe order differences with an absolute error $\delta\left(\left|\Delta N\right|\right) = 0.5$ of the fringe width, which implies the distance between neighboring bright and dark fringes. Thus, the following estimations are valid:

$$\delta\left(\left|\Delta u\right|\right) = \delta\left(\left|\Delta v\right|\right) \le 0.19\cdot 10^{-3}\ mm$$

$$\left|\delta d_{i}\right| = \sqrt{\left(\delta\left|\Delta u\right|\right)^{2} + \left(\delta\left|\Delta v\right|\right)^{2}} = 0.27\cdot 10^{-3}\ mm. \tag{15}$$

RESULTS

P ractical implementation of uncertainty analysis, presented in Section 4, needs real residual stress values inherent in investigated structures. Required data follow below.

Residual stress components in Sample 1
The mesh of probe holes drilled at the external surface of T-shaped stringer part is shown in Fig. 1 (b). The measurement points were positioned along x-direction (Line A) and along y-direction (Line B). Whole set of initial experimental data and corresponding results of residual stress determination are presented in Tab. 1. Configuration of the probe hole mesh, shown in Fig. 1 (b), indicates that locations of hole #1 and hole #6 with respect to adjacent assemblage holes are very close. Moreover, the values of hole diameter increments and principal residual stress completely coincide. Practically the same situation takes place for hole pairs #2, #7 and #3, #8. Data, which are related to the probe holes equivalently located with respect to assemblage holes, were averaged for constructing residual stress distributions. This was purposefully undertaken in order to decrease the uncertainties of residual stress components determination. The obtained results are listed in Tab.2 and Tab. 3.

Point number	ΔN^{u}, fringes	ΔN^{v}, fringes	Δu, μm	Δv, μm	σ_{1}, MPa	σ_{2}, MPa
1	−19.0	0	−7.22	0	−158.0	−53.0
2	−18.0	+1.0	−6.84	0.38	−147.0	−42.0
3	−9.5	−9.5	−3.61	−3.61	−106.0	−106.0
4	−4.0	−7.5	−1.52	−2.85	−54.0	−77.0
5	+1.0	−17.5	0.38	−6.65	−41.0	−143.0
6	−19.0	0	−7.22	0	−158.0	−53.0
7	−16.0	+1.0	−6.08	0.38	−131.0	−36.0
8	−7.5	−10.5	−2.85	−3.99	−92.0	−108.0
9	+1.0	−15.0	+0.38	−5.70	−34.0	−122.0
10	−3.0	−18.5	−1.14	−7.03	−77.0	−163.0

Table 1: Initial experimental information and values of principal residual stress components.

Point number	(1+6)/2	(2+7)/2	(3+8)/2
x, mm	3.71	10.70	20.82
σ_1, MPa	−158.0	−134.0	−99.0
σ_2, MPa	−53.0	−39.0	−107.0

Table 2: Residual stress components along Line A in Sample 1.

Point number	4	10	5	9	(8+3)/2
y, mm	1.78	3.3	6.68	9.47	14.80
σ_1, MPa	−54.0	−77.0	−41.0	−34.0	−99.0
σ_2, MPa	−74.0	−163.0	−143.0	−122.0	−107.0

Table 3: Residual stress components along Line A in Sample 1.

The spatial distribution of principal residual stress components along Line A and Line B in *Sample 1*, which are reconstructed using relations (1)-(2) and data from Tab. 2-3, is shown in Fig. 7. The origin of each axis corresponds to the edge of the nearest assemblage hole.
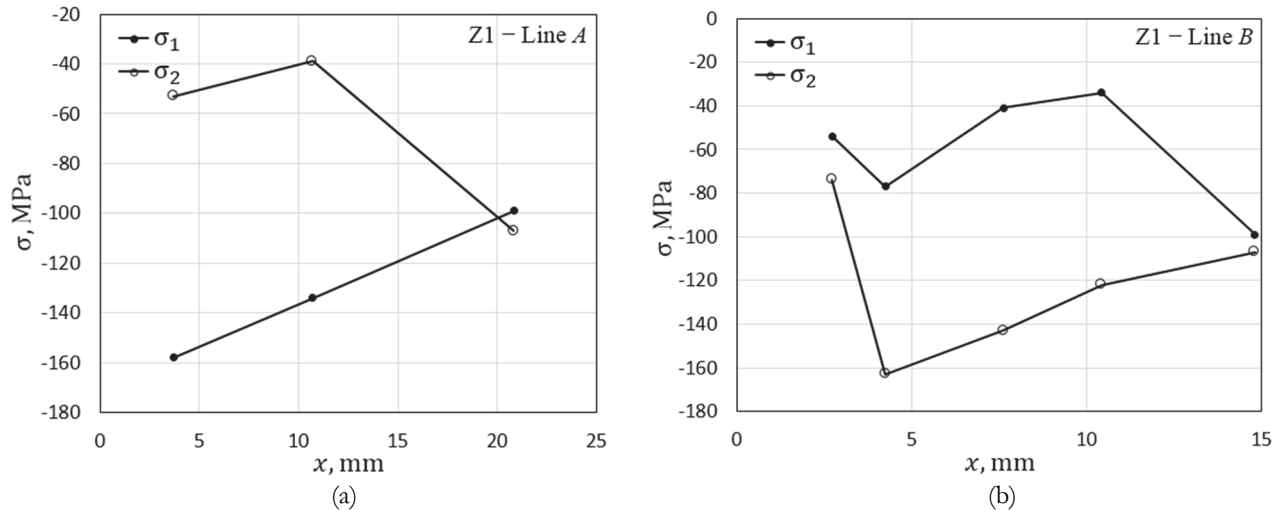

Figure 7: The principal residual stress components σ_1 and σ_2 along (a) Line A and (b) Line B in *Sample 1* as functions of distance from the nearest assemblage hole.

The findings presented in this section demonstrate practically ideal situation that might occur when residual stress determination employs a combination of blind hole drilling method and optical interferometric measurements of local deformation response. The technical parameters employed in the drilling procedure ensure high quality, resulting in precise interference fringe patterns. The maximal fringe density over a small hole diameter of $2r_0 = 1.9$ mm is 17-18 fringes, which is close to the resolution limit. The approach used facilitates the determination of principal residual stress components with values of $\sigma_1^{MIN} = -158.0$ MPa and $\sigma_2^{MIN} = -163.0$ MPa. The results indicate the development of a high-level compressive residual stress field in proximity to assembly holes subsequent to bolt removal. This unforeseen consequence offers advantages in terms of fatigue strength. It is noteworthy that a comparably designed lower wing panel underwent solely pulsed tensile loading during its fatigue testing.

Residual stress components in Sample 2
Similarly to the *Sample 1*, the configurations of fringe patterns suggest that coordinate axes x and y align with the direction of the principal residual stress components σ_1 and σ_2, respectively. It is necessary to highlight that the density of interference fringes along the probe hole edge drilled, for instance, at points PD2 and PD3 approaches the resolution limit

of the ESPI technique. The interpretations of the fringe patterns and the calculated values of the principal residual stress components, extracted from the preliminary experimental data based on formulae (1) and relations (2), are listed in Tab. 4.

Point	Distance from the edge of strengthened hole to the center of probe hole Δy, mm	ΔN^u, fringes	ΔN^v, fringes	Δu, μm	Δv, μm	σ_1, MPa	σ_2, MPa
PD1	9.16	+11.5	−14.0	+4.37	−5.32	+54.0	−80.2
PD2	3.28	+12.5	−25.0	+4.75	−9.5	+32.6	−164.5
PD3	2.54	+8.5	−24.0	+3.23	−9.12	+3.6	−169.5
PD4	9.21	+9.5	−12.0	+3.61	−4.56	+20.7	−69.7

Table 4: The results of fringe patterns interpretation and values of principal residual stress components for Sample 2.

The centres of probe holes at points PD2 and PD3 are located 3.26 mm and 2.54 mm away from the edge of the StressWave™-treated hole, respectively. The compressive residual stress components at these points are quantified as $\sigma_1 = -164.5$ MPa and $\sigma_2 = -169.5$ MPa. The residual stress values observed fall within the range of experimental uncertainty. This alignment emphasizes the uniformity of the residual stress field in the radial direction. These results are consistent with residual stress estimates obtained from a similar study using neutron diffraction methods [36].

The adopted transition model is based on the solution for elastic part of stress concentration problem in a thick plate with blind hole subjected to two-axial tension/compression under plane stress conditions [10, 23–24, 33]. Formulae (1) assume the applicability of the superposition principle to the local displacement and strain fields associated with each in-plane stress tensor components. A blind hole of diameter $2r_0$ is made at some point of the plane surface area under consideration. The centre of this hole is a conventional point, where the residual stresses must be determined. It is also assumed that a distribution of residual stress components in depth direction is uniform. This condition is valid for non-welded aluminium specimens in most of practical cases.

The plane stress conditions have been satisfied for all specimens studied as a result of the applied geometric configuration and residual stress causes. The elastic nature of the residual stress state following hole drilling can be attributed to two factors. Firstly, the fringe pattern configuration, which can be accurately resolved over the entire edge of the hole, does not exhibit any signs of plastic deformation in comparison to the example shown in Fig. 8. In this case, the interference fringe configuration highlights the presence of a two-sided indentation dimple. This is a result of blind hole drilling at point PD5.

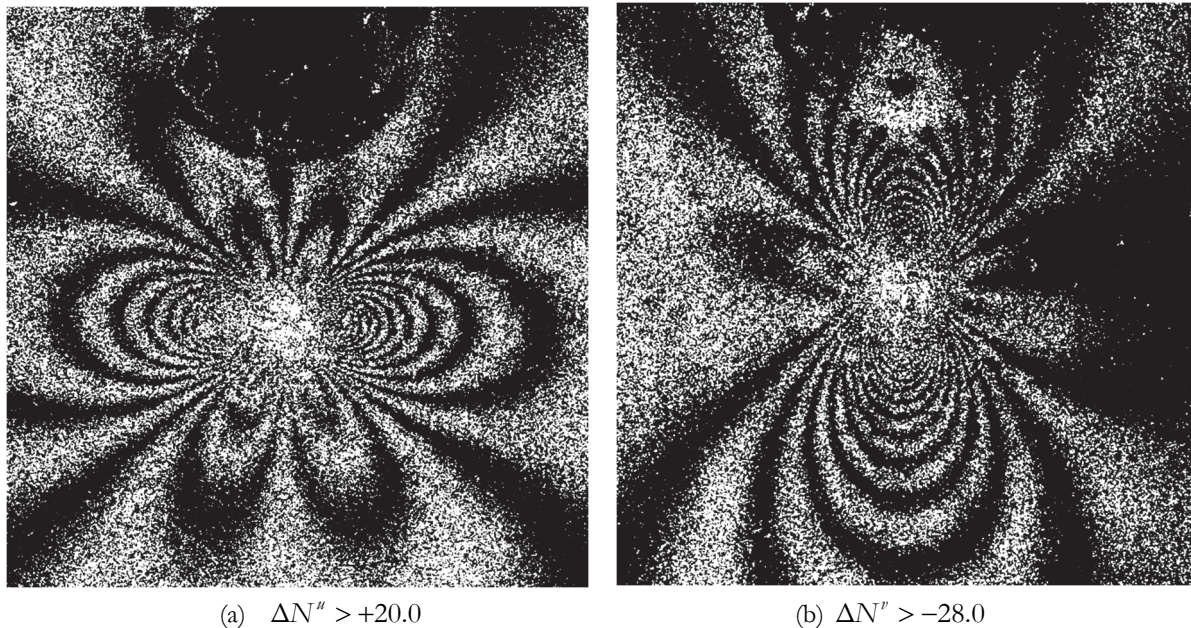(a) $\Delta N^u > +20.0$ (b) $\Delta N^v > -28.0$

Figure 8: The interference fringe patterns obtained in terms of in-plane displacement component (a) u and (b) v after drilling blind hole at point PD5.

Secondly, the largest values of principal residual stress components are $\sigma_1 = -158.0$ MPa and $\sigma_2 = -163.0$ MPa for Line A and Line B of *Sample 1*, respectively, and $\sigma_1 = -164.5$ MPa and $\sigma_2 = -169.5$ MPa for points PD2 and PD3 of Sample 2, respectively. It is obvious that the obtained residual stresses are significantly lower than the yield stress (and even 2/3 of the yield stress) of the 2024 aluminium alloy, indicating reliable determination using the blind hole drilling method [10, 40].

Uncertainty values, which follow from inequality (8), relations (13), inequality (14) and estimations (15) for experimental data in Tab. 1 and 4, are represented below in Tab. 5. The data in Tab. 5 correspond to the upper limit of experimental error in determining residual stresses, providing conservative estimates for residual stress uncertainties. This arises from the definition of the adopted Euclid matrix norm (10), as explained in reference [39]. It is worth noting, however, that this «conservative estimation» results in an absolute error in determining each principal residual stress component of 5.4 to 8.5 MPa. The relative error in determination of the maximal residual stress component fits within the range of 3.3 % to 5.3 %. This outcome, associated with a low condition number $cond\{A\}$ of 2.51, is favourable from any perspective. The presented uncertainties analysis of all experimental results requires identification of the fringe order differences with an absolute error of $\delta(|\Delta N|) = 0.5$ for the fringe width. Even with conservative assumptions, the estimated error of residual stress components determination primarily lies within the 5 % interval. This level of accuracy is sufficient to solve most engineering problems. However, automated procedures for in-plane displacement filed acquisition can greatly enhance accuracy if necessary.

Specimen	Point	σ_1, MPa	σ_2, MPa	s, MPa	d 10^{-3}, mm	$\delta(\sigma_1)$, MPa	$\delta(\sigma_2)$, MPa	$\dfrac{\delta(\sigma_1)}{\sigma_1}$	$\dfrac{\delta(\sigma_2)}{\sigma_2}$
Sample 1,	10	−77.0	−163.0	180.3	7.19	8.50	8.50	0.11	0.047
Line B	5	−41.0	−143.0	148.8	6.66	7.57	7.57	0.18	0.053
Sample 2	PD2	+32.6	−164.5	167.7	10.6	5.36	5.36	0.16	0.033

Table 5: Uncertainties estimations for several specific points for two samples.

DISCUSSION

Most of currently used blind hole drilling techniques for residual stress determination are based on the multiple-point over-deterministic approach. In these cases, matrix A from Eqns. (5) and (6) is a rectangular $(m \times n)$ matrix with $m > n$, i.e. $s = \{s_n\}$ and $d = \{d_m\}$. Thus, the problem becomes overdetermined and improperly posed (ill-posed). In general, no solution exists. However, as a rule, the measured data d are full of errors (ε), thus Eqn. (6) can be written as given earlier [30]:

$$A \cdot s = d + \varepsilon \tag{16}$$

It means that solution can be found via adjustment of least squares thereby minimizing the quadratic functional:

$$J = \sum_{i=1}^{m} \left(\sum_{j=1}^{n} A_{ij} \cdot s_i - d_i \right)^2 = A \cdot s - d^2 \rightarrow min \tag{17}$$

Therefore, the solution corresponding to (17) can be found via:

$$s = \left(A^T \cdot A \right)^{-1} \cdot A^T \cdot d \tag{18}$$

Recent research [32] provides a thorough analysis of how Eqns. (16)-(18) can be used to determine residual stress via the hole drilling method. The study highlights that "measured parameters at any given increment, determined by the cumulative effect of the relieved stresses, appear as an integral equation, which must be inverted to obtain residual stresses. In practice,

stress distributions are discretized by a finite-dimensional basis, to transform the integral equations into a linear system of equations, which is often ill-conditioned. The inversion of the integral equations arising from relaxation methods is an *ill-posed* problem, which is a very specific mathematical property and must be distinguished from a general *ill-conditioning*. Ill-posed problems require additional assumptions to obtain a physically meaningful solution. This process falls under the name of *regularization*".

Many studies focused on determining residual stress in hole drilling implement overly complex methods, such as multiple-points over-deterministic procedures involving calibration coefficient calculations and solving ill-conditioned systems of linear algebraic equations. However, non-equality (8) indicates that determining residual stress has no practical sense if $cond\{A\} \geq 10$. It is worth nothing that condition number values are not taken into account in several papers devoted to this problem. It appears that many of the linear algebraic systems are ill-conditioned, thus requiring further efforts to achieve reliable residual stress evaluation. For instance, this problem can be partially solved by regularization techniques, but they only provide incidental uncertainty estimation.

Our approach can be defined as "preventive regularization", which aids in eliminating the aforementioned difficulties. The application of two measurement points for determination of hole-diameter increments along principal stress directions yields an unequivocal solution to the properly posed inverse problem as described in Eqn. (6). An explicit form of this solution is given in Eqn. (1). It employs the solution of linear algebraic equations system with low condition number $cond\{A\} = 2.51$. Very optimistic estimations of errors inherent to the final results directly follow from relationships (8)-(18), and they prove main advantages of the developed approach clearly.

It would be very useful to review the challenges outlined in the conclusions section of the fundamental paper by G.S. Schajer, M.B. Prime, and P.J. Withers [5] with respect to the approach presented in this article. We summarize our answers in Tab. 6.

Challenge from paper [5]	Answer
1. The need for an absolute zero-stress datum. This is often difficult to achieve in practice. For relaxation type measurements, highly accurate, stress-free cutting is essential. … **2.** The sample may need to be physically damaged in order to make the measurements. Such damage occurs with all relaxation type measurements, and sometimes also with diffractive measurements. …	**I–II**. All probe holes are made using a hard-coated drill. The rotational speed is fixed at 60 rpm, and the translation speed of the drill does not exceed 0.125 mm/sec. This technology allows for highly precise stress-free local material removal without physical damages, as depicted in Fig. 9. The uniform stress field inherent in the middle plane of the end face of *Sample 1* is shown in Fig. 10. It is important to note that the residual stress values closely match those obtained at points 3 and 8 on the exterior surface (refer to Tab. 1). Thus, we clearly illustrate how to acquire both absolute zero-stress and non-zero-stress datum.
4. Sensitivity to stresses at nearby locations in addition to those at the measurement location. This issue typically creates the need for "inverse" calculations.	**IV**. Stress evaluations in nearby areas and "inverse" calculations are not necessary since the initial experimental data is immediately obtained at the hole edge. The center of probe hole is a conventional point to which obtained residual stress components are referred. Measurement of deformation response to local material removal directly at the hole edge provides maximal possible sensitivity with respect to residual stress determination.
5. Substantial sensitivity to measurement and procedural imperfections. Consequently, a very high standard of measurement and procedural precision is required to achieve effective results.	**V**. Absolute error that is inherent in the determination of each principal residual stress component, as indicated by inequality (8), directly quantifies significant sensitivity to measurement imperfections. The high quality of the interference fringe patterns effectively demonstrates the robustness of the experimental procedure. This signifies that a very high standard of measurement and procedural precision is necessary to yield efficient results.

Table 6: Challenges manifested in reference [5] and responses to them.
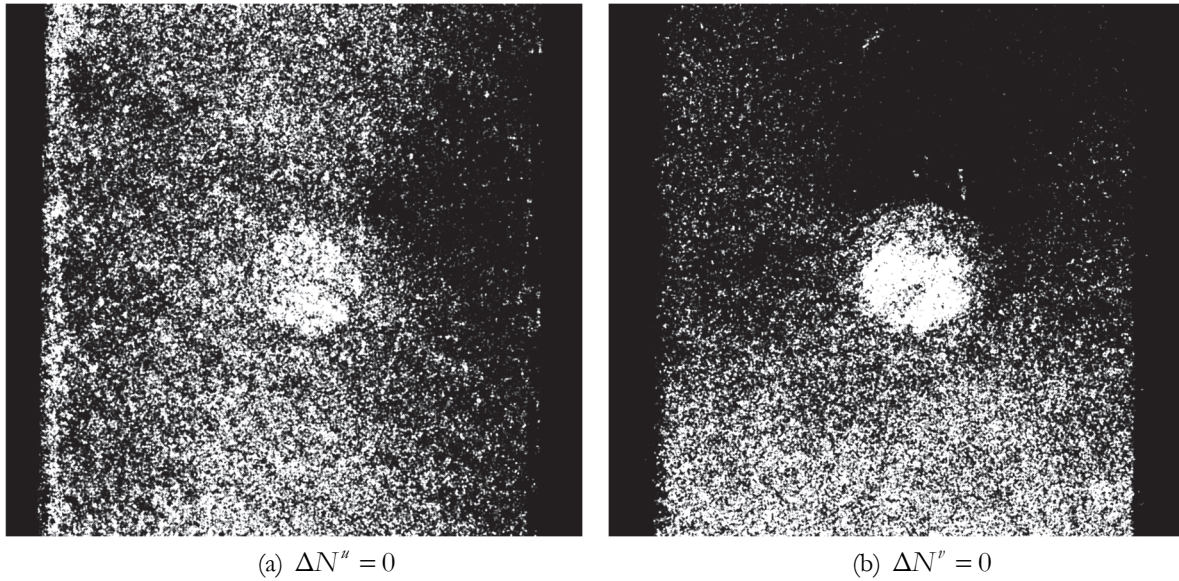
(a) $\Delta N^u = 0$ (b) $\Delta N^v = 0$

Figure 9: Zero-stress level ($\sigma_1 = \sigma_2 = 0$) revealed on the end face of *Sample 2* after drilling deep blind hole. In-plane displacement component (a) u and (b) v.
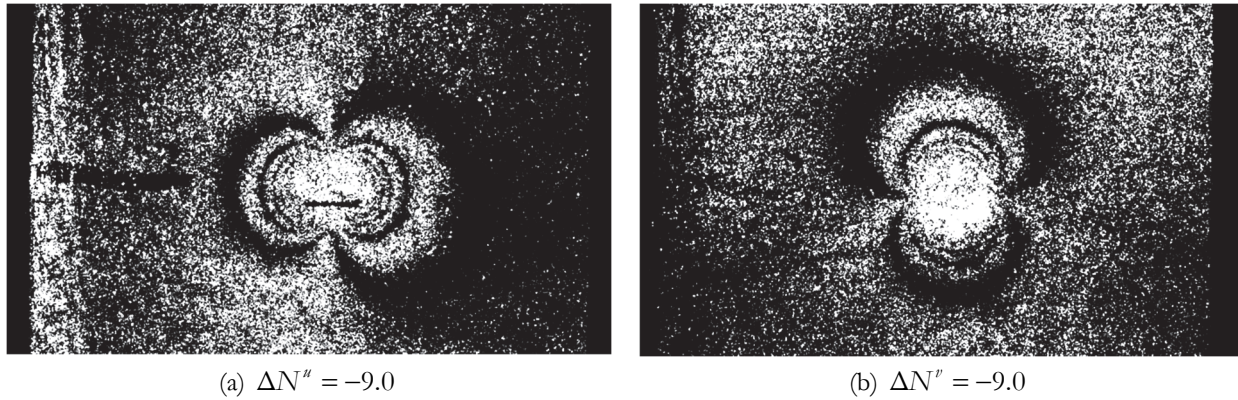

(a) $\Delta N^u = -9.0$ (b) $\Delta N^v = -9.0$

Figure 10: Uniform stress level ($\sigma_1 = \sigma_2 = -100.0$ MPa) revealed on the end face of *Sample 1* after drilling deep blind hole. In-plane displacement component (a) u and (b) v.

Arguments presented in Tab. 6 demonstrate that all challenges outlined in reference [5] have been successfully addressed. Additionally, an unmentioned challenge related to "the inversion of the integral equations arising from relaxation methods is an *ill-posed* problem" [32] has also been overcome.

Moreover, in this study we demonstrated a high-quality data collection with sufficient level of accuracy that is essential for most engineering problems. However, the achieved accuracy of residual stress determination can be reinforced through numerical simulation and corresponding visualization of reference fringe patterns that arise during blind hole drilling [23, 24, 40]. On the other hand, automated procedures for in-plane displacement filed acquisition can greatly enhance accuracy as well.

Below, we will provide a first attempt in this direction. The analytical Kirsch solution around a circular hole in an infinite plate rewritten for displacements can be used for this task [42]:

$$u_r = \frac{1}{2G}\left\{\frac{1}{2}\left(p_x + p_y\right)\frac{R^2}{r} + \frac{1}{2}\left(p_x - p_y\right)\left[4(1-v)\frac{R^2}{r} - \frac{R^4}{r^3}\right]\cos 2\varphi\right\}$$

$$u_\varphi = -\frac{1}{4G}\left(p_x - p_y\right)\left[2(1-2v)\frac{R^2}{r} + \frac{R^4}{r^3}\right]\sin 2\varphi \tag{19}$$

where u_r are radial displacements, u_φ are tangential displacements, G is shear modulus of the material, p_x and p_y are principal stresses along x- and y-axis, respectively, ν is Poisson's ratio of the material, R is radius of the hole.

The results for the $\sqrt{u_r^2 + u_\varphi^2}$ analytical solution (with the addition of simulated noise) are shown in Fig. 11 in comparison with the experimentally obtained interference fringe pattern from Fig. 3 (a). The illustration provides a demonstration of the possibility for developing a correlation-based analysis approach (pattern matching) that will be the subject of a separate future study.

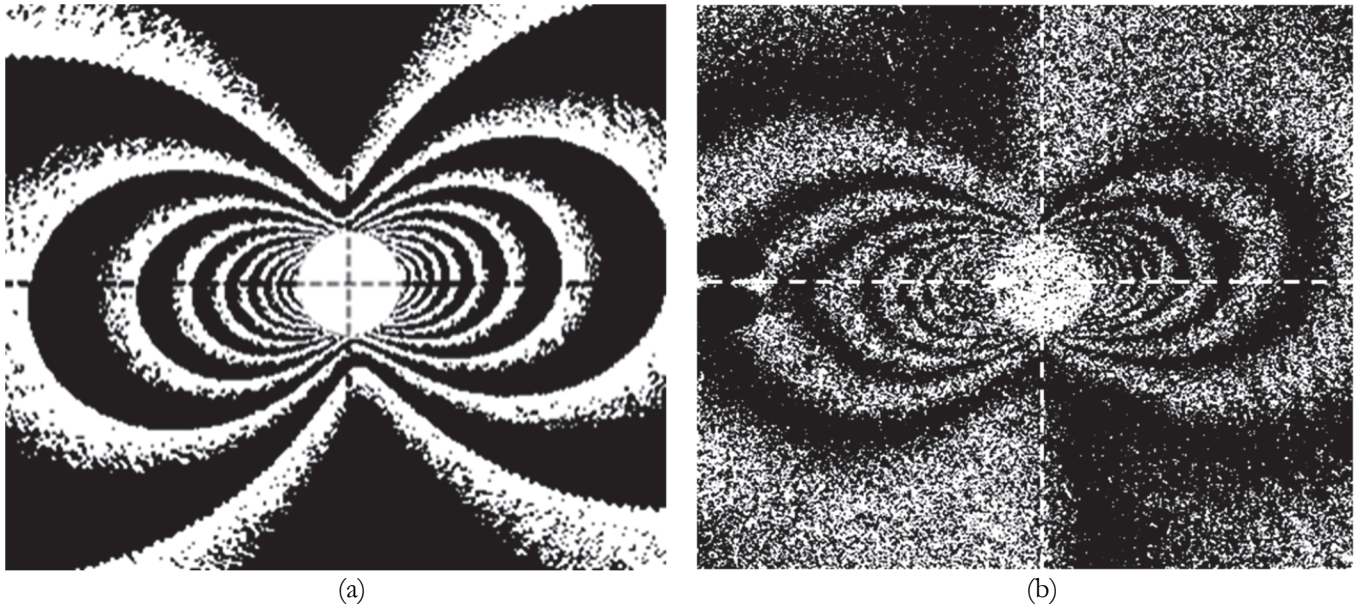(a)   (b)

Figure 11: (a) The simulated fringe pattern obtained from the Kirsch solution for displacements around a circular hole in an infinite plate compared with (b) the experimentally obtained interferometry fringe pattern.

CONCLUSIONS

In this study, we have conducted experiments to determine residual stress from blind deep hole drilling in thick plates using electronic speckle-pattern interferometry, which is based on the measurements of probe hole diameter increments along principal strain directions. Moreover, we have developed an efficient experimental procedure that includes local deformation parameters which can be measured with the highest possible accuracy. Hole diameter increments along directions of principal strains, precisely represent the parameters that satisfy the above-mentioned conditions. Derived formulae, which provide the transition from raw experimental data to required values of principal residual stress components, are the unequivocal solutions to the properly posed inverse problem. Thus, there is no need to apply various regularization procedures to enhance the reliability of residual stress determination.

The accuracy of the proposed approach for the residual stress components determination has been analytically assessed. It was found that the absolute error of each principal residual stress component lies in the range of 5.4 to 8.5 MPa depending on the type of residual stress field considered. Corresponding relative errors range from 3.3 % to 5.3 % when the value of maximal negative residual stress component is altered from -164.5 to -143.0 MPa, respectively. This remarkably low level of uncertainty is achieved, even when considering that the differences in fringe order were derived with the half accuracy of the absolute fringe order.

The accuracy demonstrated by the proposed technique is more than satisfactory for most engineering problems. The developed approach is significantly important for the fast and reliable characterization of high-level residual stresses that arise in irregular zones of thick-walled structures. The experimental procedure is straightforward and does not require a highly skilled practitioner to achieve successful results.

ACKNOWLEDGEMENTS

REFERENCES

[1] Masubuchi, K. (1980). Analysis of welded structures: residual stresses, distortion, and their consequences. Pergamon: Oxford.

[2] Withers, PJ., Bhadeshia HKDH. (2001). Residual stress: Part 1 - measurement techniques, Mater Sci Technol, 17, pp. 355–365.

[3] Schajer, GS. (2001). Residual stresses: Measurement by destructive methods. In: Buschow KHJ, et al. (eds) Encyclopedia of Materials: Science and Technology, Section 5a, Elsevier Science, Oxford.

[4] Schajer, GS (ed). (2013). Practical residual stress measurement methods. Wiley, Chichester, UK.

[5] Schajer, GS., Prime, MB., Withers, PJ. (2022). Why Is It So Challenging to Measure Residual Stresses?, Experimental Mechanics, 62, pp. 1521-1530, DOI: 10.1007/s11340-022-00879-x.

[6] Nelson, DV. (2010). Residual stress determination by hole drilling combined with optical methods, Exp. Mech., 50(2), pp. 145–158, DOI: 10.1007/s11340-009-9329-3.

[7] Schajer, GS. (2010). Advances in hole-drilling residual stress measurement, Exp. Mech., 50(2), pp. 159–168, DOI: 10.1007/s11340-009-9228-7.

[8] Huang, X., Liu, Z., Xie, H. (2013). Recent progress in residual stress measurement techniques, Acta Mech Solida Sin, 26(6), pp. 570–583, DOI: 10.1016/S0894-9166(14)60002-1.

[9] Jiang, G., Fu, H., Pan, B., Kang, R. (2019). Recent progress of residual stress measurement methods: A review. Chinese Journal of Aeronautics, 34(2), pp. 54-78, DOI: 10.1016/j.cja.2019.10.010.

[10] Pisarev, V.S., Odintsev, I.N., Eleonsky, S.I., Apalkov, A.A. (2018). Residual stress determination by optical interferometric measurements of hole diameter increments, Optics and Lasers in Engineering, 110, pp. 437–456, DOI: 10.1016/j.optlaseng.2018.06.022.

[11] Nelson, D.V., Fuchs, E.A., Makino, A., Williams, D.R. (1994). Residual stress determination by single axis holographic interferometry and hole drilling - Part II, Experiments. Exp Mech, 34(1), pp. 79–88, DOI: 10.1007/BF02328444.

[12] Nelson, D.V., Makino, A., Fuchs, E.A. (1997). The holographic hole-drilling method for residual stress determination, Opt. Lasers Eng., 27(1), pp. 3–23.

[13] Makino, A., Nelson, D.V., Fuchs, E.A., Williams, D.R. (1996). Determination of biaxial residual stresses by a holographic hole-drilling technique, ASME J. Eng. Mater. Technol., 118(4), pp. 583–538.

[14] Steinzig, M., Ponslet, E. (2003). Residual stress measurement using the hole drilling method and laser speckle interferometry –Part I, Exp. Tech., 27(3), pp. 43–46, DOI: 10.1111/j.1747-1567.2003.tb00114.x.

[15] Ponslet, E., Steinzig. M. (2003). Residual stress measurement using the hole drilling method and laser speckle interferometry - Part II: Analysis technique, Exp. Tech., 27(4), pp. 1–5, DOI: 10.1111/j.1747-1567.2003.tb00117.x.

[16] Ponslet, E., Steinzig, M. (2003). Residual stress measurement using the hole drilling method and laser speckle interferometry - Part III: Analysis technique, Exp. Tech., 27(5), pp. 45–48, DOI: 10.1111/j.1747-1567.2003.tb00130.x.

[17] Steinzig, M., Takahashi, T. (2003). Residual stress measurement using the hole drilling method and laser speckle interferometry - Part IV: Measurement accuracy, Exp. Tech., 27(6), pp. 59–63, DOI: 10.1111/j.1747-1567.2003.tb00141.x.

[18] Schajer, G.S., Steinzig, M. (2005). Full-field calculation of hole drilling residual stresses from electronic speckle pattern interferometry data, Exp. Mech., 45(6), pp. 526–532, DOI: 10.1007/BF02427906.

[19] Schmitt, D.R., Hunt, R.W. (2000). Inversion of speckle interferometer fringes for hole drilling residual stress determination, Exp. Mech., 40(2), pp. 1–9, DOI: 10.1007/BF02325038.

[20] Schajer, G.S., Prime, M.B. (2006). Use of inverse solutions for residual stress measurement, ASME J. Eng. Mater. Technol., 128(3), pp. 375–382, DOI: 10.1115/1.2204952.

[21] Furgiuele, F.M., Pagnotta, L., Poggialini, A. (1991). Measuring residual stresses by hole drilling and coherent optics techniques: a numerical calibration, ASME. J. Eng. Mater. Technol., 113(1), pp. 41–50.

[22] Ruzman, I., Schmitt, D.R. (2003). Three-dimensional stress-relief displacements from blind–hole drilling: a parametric description, Exp. Mech., 43(1), pp. 52–60, DOI: 10.1007/BF02410484.

[23] Pisarev, V.S., Balalov, V.V., Aistov, V.S., Bondarenko, M.M., Chumak, S.V., Grigoriev, V.D., Yustus, M.G. (2004). Metrological justification of reflection hologram interferometry with respect to residual stresses determination by means of blind hole drilling, Opt. Lasers Eng., 41(2), pp. 353–410, DOI: 10.1016/S0143-8166(02)00212-9.

[24] Pisarev, V.S., Balalov, V.V. (2004). A role of fringe pattern catalogue in the course of interferometrically based determination of residual stresses by the hole-drilling method, Opt. Lasers Eng., 41(2), pp. 411–462, DOI: 10.1016/S0143-8166(02)00203-8.

[25] Schajer, G.S., Winiarski, B., Withers, P.J. (2013). Hole-drilling residual stress measurement with artifact correction using full-field DIC, Exp. Mech., 53(2), pp. 255–265, DOI: 10.1007/s11340-012-9626-0.

[26] Baldi, A. (2014). Residual stress measurement using hole drilling and integrated digital image correlation techniques, Exp. Mech., 54(3), pp. 379–391, DOI: 10.1007/s11340-013-9814-6.

[27] Harrington, J.S., Schajer, G.S. (2017). Measurement of structural stresses by hole-drilling and DIC, Exp. Mech., 57(4), pp. 559–567, DOI: 10.1007/s11340-016-0247-x.

[28] Hagara, M., Trebuňa, F., Pastor, M., Huňady, R., Lengvarsky, P. (2019). Analysis of the aspects of residual stresses quantification performed by 3D DIC combined with standardized hole-drilling method, Measurement 29, 137, pp. 238–256, DOI: 10.1016/j.measurement.2019.01.028.

[29] Statnik, E.S., Uzun, F., Lipovskikh, S.A., Kan, Y.V., Eleonsky, S.I., Pisarev, V.S., Somov, P.A., Salimon, A.I., Malakhova, Y.V., Seferyan, A.G., et al. (2021). Comparative Multi-Modal, Multi-Scale Residual Stress Evaluation in SLM 3D-Printed Al-Si-Mg Alloy (RS-300) Parts, Metals, 11, 2064, DOI: 10.3390/met11122064.

[30] Laermann, K.H. (2001). Reliable evaluation of measured data – an inverse problem. In: Juptner W, Osten W, editors. Fringe 2001–Proceedings of the 4th international workshop on automatic processing of fringe patterns. Paris: Elsevier, pp. 443–500.

[31] Prime, M.B., Hill, M.R. (2006). Uncertainty, model error, and order selection for series-expanded, residual-stress inverse solutions, J. Eng. Mater. Technol., 128(2), pp. 175–185, DOI: 10.1115/1.2172278.

[32] Beghini, M., Grossi, T., Prime, M.B., Santus, C. (2022). Ill-posedness and the bias-variance trade off in residual stress measurement inverse solutions, Exp. Mech., 62, pp. 1-11, DOI: 10.1007/s11340-022-00928-5.

[33] Pisarev, V.S., Grigoriev, V.D., Balalov, V.V., Chumak, S.V. (2004). Residual stresses deriving from holographic interferometry data on a base of inverse problem solution, Optics & Lasers in Engineering, 42(6), pp. 703-726, DOI: 10.1016/j.optlaseng.2004.05.003.

[34] Pisarev, V.S., Bondarenko, M.M., Chernov, A.V., Vinogradova, A.N. (2005). General approach to residual stresses determination in thin-walled structures by combining the hole drilling method and reflection hologram interferometry, International Journal of Mechanical Sciences, 47(9), pp. 1350–1376, DOI: 10.1016/j.ijmecsci.2005.05.002.

[35] Easterbrook, E.T., Flinn, B.D., Meyer, C., Juhlin, N. (2001). The StressWave Fatigue Life Enhancement Process. Proceedings of the 2001 Aerospace Congress.

[36] Flinn, B., Wiegman, M., Landy, M., Nam, T., Easterbrook, E. (2004). Stresswave® fatigue life improvement process, SAE Technical Paper.

[37] Boni, L., Fanteria, D., Lanciotti, A., Polese, C. (2013). Experimental and analytical assessment of fatigue and crack propagation in cold worked open hole specimens, Fatigue Fract. Engng. Mater. Struct., 36, pp. 930–941, DOI: 10.1111/ffe.12050.

[38] Robinson, J., Ashton, I., Fox, P., Jones, E., Sutcliffe, C. (2018). Determination of the effect of scan strategy on residual stress in laser powder bed fusion additive manufacturing, Additive Manufacturing, 23, pp. 13–24, DOI: 10.1016/j.addma.2018.07.001.

[39] Montero, J., Weber S., Bleckmann, M., Paetzold, K., Jagle, E. A. (2022). Determination of bi-dimensional normal residual stress distributions in metallic laser-based powder bed fusion parts, Mechanics of Materials, 173, 104437, DOI: 10.1016/j.mechmat.2022.104437.

[40] Pisarev, V.S., Balalov, V.V., Aistov, V.S., Bondarenko, M.M., Yustus, M.G. (2001). Reflection hologram interferometry combined with hole drilling technique as an effective tool for residual stresses fields investigation in thin-walled structures, Opt. Laser Eng., 36, pp. 551–597, DOI: 10.1016/S0143-8166(01)00065-3.

[41] Lankaster, P. (1969). Theory of Matrices; Academic Press: New York, London.

[42] Timoshenko, S., Goodier, J. (1970). Theory of Elasticity. New-York: McGraw-Hill.